Environmental Science & Technology

pubs.acs.org/est

Article

Open Access

This article is licensed under CC-BY 4.0

Photoinduced Intraparticle Chemistry Drives the Rapid Atmospheric Oxidation of Biomass Burning Organic Aerosol

Jun Zhang, Rico K. Y. Cheung, Zachary C. J. Decker, Mihnea Surdu, Sophie Bogler, Kun Li, Tiantian Wang, Robin L. Modini, Jay G. Slowik, Demetrios Pagonis, Hongyu Guo, Pedro Campuzano-Jost, Jose L. Jimenez, Matthew M. Coggon, Georgios I. Gkatzelis, Carsten Warneke, Samuel R. Hall, Kirk Ullmann, Glenn S. Diskin, Joshua P. Digangi, Jeff Peischl, Christopher D. Holmes, Shan Zhou, Qi Zhang, David M. Bell,* Imad El Haddad,* and Andre S. H. Prevot*

Cite This: *Environ. Sci. Technol.* 2026, 60, 24206−24216

Read Online

ACCESS | Metrics & More | Article Recommendations | Supporting Information

ABSTRACT: Biomass burning (BB) is the second largest global source of organic aerosol (OA), with its impact on climate and air quality expected to rise with global warming. Aircraft measurements of BB plumes show a rapid increase in the OA oxidation state, which could not be reproduced in simulation chambers based on gas-phase oxidation. Here, we investigate isolation key aging processes of BB emissions in controlled chamber experiments, including the effects of ultraviolet-A irradiation, OH-driven secondary OA formation, heterogeneous OH oxidation or ozonolysis, and evaporation. We find that ultraviolet-A irradiation can drive rapid intraparticle OA aging within hours, proceeding an order of magnitude faster than gas-phase oxidation. Other mechanisms were even slower in producing oxygenated OA (OOA). Based on our experiments, we estimate that this process proceeds with a quantum yield of ∼0.4%, meaning that four in every thousand photons absorbed by organic chromophores in BBOA generate radicals in the particle phase that rapidly oxidize the particulate organics. We further analyzed aircraft measurements of wildfire and prescribed burn plumes, showing that photoinduced processes can account for much of the rapid OOA formation. We estimate that, in BB-influenced regions, over half of OOA may originate from photo-oxidized primary OA within the first day. Our findings challenge the prevailing paradigm that gas-phase oxidation dominates BBOA aging and highlight a previously underappreciated, but dominant role of intraparticle photochemistry.

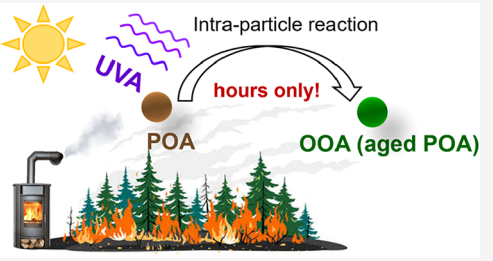

KEYWORDS: *biomass burning organic aerosol, oxygenated organic aerosol, photoinduced intraparticle chemistry*

INTRODUCTION

Biomass burning (BB) releases roughly 4.9 Tg of black carbon and 36 Tg of primary organic aerosol (POA) annually,[1] with their impact on Earth's climate and human health[2,3] expected to rise with global warming,[4,5] primarily due to more frequent heat waves and drought conditions. In the atmosphere, these emissions undergo complex physical and chemical changes, including evaporation of semivolatile compounds,[6] generation of secondary organic aerosol (SOA) through oxidation of reactive gases followed by gas-to-particle conversion,[7] and heterogeneous reactions of POA.[8] These processes may increase the oxidation level of BBOA, altering their optical properties, hygroscopicity, and oxidative potential, thereby affecting their effects on climate and health.

A key indicator of aerosol oxidation is the fraction of m/z 44 (CO_2^+), f_{44}, in aerosol mass spectrometer (AMS) measurements, which originates from highly oxygenated compounds and reflects the most oxidized form of carbon. f_{44} correlates with oxygen-to-carbon ratio (O/C) and carbon oxidation state (OS_C).[9] In winter, elevated levels of oxygenated organic aerosols (OOA) marked by high f_{44} and O/C values are commonly observed at urban locations near emissions.[10−13] While part of this OOA arises from SOA formed by gas-phase oxidation of anthropogenic precursors,[12] a substantial fraction is often traced back to aged BBOA.[14] However, the speed at which this OOA forms under limited oxidative conditions presents a persistent atmospheric conundrum.[15] Airborne measurements show that wildfire plumes can also undergo rapid oxidation, with f_{44} increasing up to 3-fold within hours.[16−19] Agricultural burns display a comparable trend, with a sharp rise in O/C ratios from ∼0.4 to as high as 0.8 in under an hour.[20] This oxidation has often been ascribed to the evaporation of semivolatile species and followed by hydroxyl radical (OH)-initiated gas-phase oxidation and partitioning of oxidation products. Yet, laboratory studies reveal that OH-

Received: February 13, 2026
Revised: July 1, 2026
Accepted: July 2, 2026
Published: August 21, 2026



ACS Publications

© 2026 The Authors. Published by American Chemical Society

Downloaded from pubs.acs.org/esthag/article-pdf/60/34/24206/6704211/acs.est.6c02532.pdf by FORSCHUNGZENTRUM JUELICH user on 26 November 2026

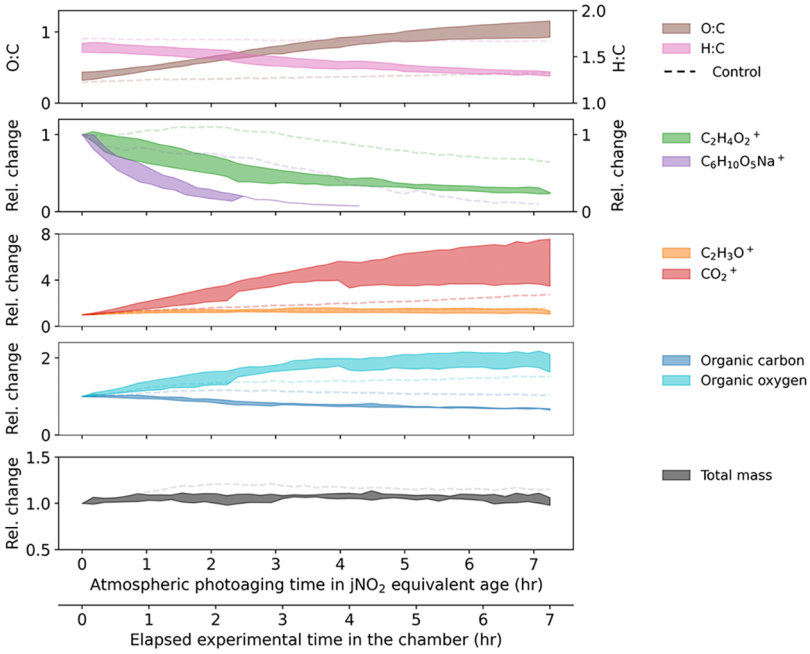

Figure 1. Time series of elemental ratios, ions, and total organic carbon and oxygen of OA originating from spruce residential burning when exposed to UVA radiation. The changes in ions, total organic carbon mass, and total organic oxygen mass are shown as relative changes (Rel. change) from the start of radiation. The elemental ratios using the method from Canagaratna et al.[9] and ions are quantified with AMS. The total organic carbon mass is calculated from AMS fragments containing carbon, and the total organic oxygen mass is calculated from AMS fragments containing oxygen. $C_6H_{10}O_5Na^+$ was measured with EESI-TOF. The shaded areas represent the standard deviation from five repeat experiments, except for $C_6H_{10}O_5Na^+$, which was measured in three replicates. When the standard deviation could not be calculated due to the limited number of measurements, the data are shown as a solid line instead of a shaded area. The dashed lines represent the average of the time series observed from two dark ozonolysis experiments, considered as control experiments (i.e., same experimental conditions but without UVA light). The photolysis rate of NO_2 (jNO_2) in this smog chamber is $2.9 \times 10^{-3} \pm 1 \times 10^{-4}$ s^{-1}. The atmospheric photoaging time in jNO_2 equivalent age is calculated by dividing the accumulative jNO_2 in the chamber by the 24 h average jNO_2 in the ambient atmosphere, assuming 2.8×10^{-3} s^{-1}, which is the average of jNO_2 summer and winter in Boulder, Hyytiälä, and at the Equator.[31] The average of jNO_2 is meant to align with the concept of the 24 h ambient average OH (discussed later), so that these two can be compared when discussing the aging time. Particles emitted from open burning exhibit the same trend as shown in Figure S3.

driven SOA formation from BB emissions requires multiple generations of oxidation,[21] proceeding simply too slowly to account for the oxidation rates observed in the field,[22−25] exposing a fundamental gap in the current understanding of BBOA aging pathways. At the same time, a growing body of experiments primarily based on simplified BBOA surrogates has shown that light absorption can generate OH radicals, singlet oxygen ($^1O_2$), and triplet-state carbonyls ($^3C^*$), capable of oxidizing BBOA in the particle phase.[26−29] However, how these photoinduced intraparticle reactions alter the chemical composition of BBOA and how rapidly it proceeds remains unclear.

Here, we combine an atmospheric simulation chamber and an oxidation flow reactor (OFR) to isolate and compare key aging processes of BB emissions from residential log combustion and open burning of fresh conifer wood. Using an AMS, we track the evolution of OA oxidation state during both gas-phase OH oxidation and intraparticle photoinduced oxidation. We show, for the first time, that photoinduced processes within the particle phase led to substantially faster oxidation than traditional gas-phase pathways. By following the rapid decay of levoglucosan, a tracer for fresh BB emissions, we provide evidence that this process involves radical chemistry within the particle phase. Finally, by reanalyzing airborne observations from wildfire and prescribed burn plumes, we demonstrate that intraparticle photoinduced aging can explain the unexpectedly rapid BBOA oxidation often observed in the atmosphere.

METHODS

Laboratory Simulation of BB Emission Aging

The experiments were carried out at the Paul Scherrer Institute (PSI) in the PSI Atmospheric Simulation Chambers and Reactors (PACs). The experimental setup is shown in Figure S1. Spruce logs were burned in a stove to simulate residential burning, and fresh spruce and pine branches were burned in a top-open stainless-steel drum to mimic open burning fires. The residential stove is an iron-cast model (Invicta Remilly, P601384), operated with the door closed during combustion. The emissions were delivered to a Teflon environmental chamber (~8 m^3) using an ejector dilutor (DI-1000, Dekati Ltd.) with a dilution ratio of approximately 10 via a heated stainless-steel line (180 °C). The elevated temperature of the injection line can minimize the emission loss caused by the large temperature difference between the stove and sampling line. This temperature does not alter the chemical composition, as it is below the typical combustion temperature. Before emissions entered the chamber, the gas-phase species were stripped using charcoal denuders (Ionicon), which can remove gaseous organic compounds with 99% efficiency while maintaining limited particle loss, ensuring that only particles were introduced into the chamber for further analysis.[30] After the POA concentration reached around 100 $\mu g/m^3$, the injection stopped, and POA was mixed in the chamber at 20 °C for over 30 min for subsequent photoinduced aging experiments. In the photoinduced aging experiments, POA was irradiated with evenly distributed UVA (λ = ~365 nm) lamps (Cleo Performance, Philips) for ~7 h (see

Downloaded from pubs.acs.org/esthag/article-pdf/60/34/24206/6704211/acs.est.6c02532.pdf by FORSCHUNGZENTRUM JUELICH user on 26 November 2026

https://doi.org/10.1021/acs.est.6c02532
Environ. Sci. Technol. 2026, 60, 24206−24216

Table S1). Three milliliters of methanol (HPLC-grade, Sigma-Aldrich) (~226 ppm in the chamber) was injected into the chamber as an OH scavenger through the heated line with purging air for a subset of photoinduced aging experiments, mitigating any potential OH radicals generated in the chamber.

The radiation intensity in the chamber was quantified using actinic flux, represented by the photolysis frequency of NO_2 (jNO_2), which aligns with the chamber's UVA range. The photoaging time, expressed as jNO_2 equivalent age, was calculated by dividing the cumulative chamber jNO_2 by the 24-h average ambient jNO_2 (2.8×10^{-3} s^{-1}) based on average observations from Boulder (USA), Hyytiälä (Finland), and at the Equator,[31] which is comparable to the chamber jNO_2 (2.9×10^{-3} s^{-1}).

Alternatively, the emission was delivered to a holding tank (stainless steel, 1 m^3) without removal of the gas-phase species. The holding tank served as a reservoir to continuously provide primary emissions downstream. After the emissions were mixed, gases and particles were introduced to an OFR,[32] where the OH-induced oxidation took place. The detailed description can be found in the SI.

Particle concentration was monitored using a scanning mobility particle sizer (SMPS, model 3938, TSI) scanning a range of 16 to 638 nm in the particle mobility diameter. The chemical composition of POA and OA during the aging processes stated above was measured in real-time by a high-resolution time-of-flight AMS (Aerodyne Research, Inc.) and at times with an extractive electrospray ionization time-of-flight mass spectrometer[33] (EESI-TOF, Tofwerk). The EESI-TOF measured water-soluble oxygenated organic aerosols at the molecular formula level and was primarily used to monitor the abundance of levoglucosan. The EESI-TOF signal exhibits a linear response to the mass of levoglucosan.[34] A detailed description of AMS and EESI-TOF can be found in the SI and literature.[33,35]

Aircraft Measurement of BB Plumes and Chemical Age Estimation

Information and data from the Fire Influence on Regional to Global Environments and Air Quality (FIREX-AQ) campaign can be found in the work of Warneke et al.,[36] and specific instrument and fire information used here can be found in the work of Decker et al.[37] and SI. The OH exposure of FIREX-AQ was constrained using the ratio of phenol and benzene, which are directly emitted from fire and dominantly oxidized by OH. The detailed calculation can be found in the work of Xu et al.[38] The plume's jNO_2 exposure accounts for changes in ambient light intensity as the plume ages. It was assumed that the plume's extinction coefficient was constant during aging, and then that extinction factor was applied to clear-sky estimates of jNO_2 from the NCAR TUV calculator (https://www.acom.ucar.edu/Models/TUV/Interactive_TUV/tuv-x.shtml, last access 18th February, 2025) for the time period between emission and sampling.

The case study of forest fire by Morgan et al.[18] was sampled by flight B737 in the campaign of South American Biomass Burning Analysis (SAMBBA) on September 20, 2012, in Rondônia state, Brazil. The sampling time was from 11:45 to 13:30 local time. The OH exposure was simply estimated by assuming the OH daytime exposure of 2.2×10^6 molecular/cm^3 which has been observed in tropical rainforests at noontime.[39] Its jNO_2 exposure was estimated using the TUV model.

RESULTS

Rapid Aging of BB POA Initiated by Ultraviolet-A (UVA) Radiation

Dried spruce logs and fresh spruce and pine were burned in a stove and open air to simulate residential burning and wildfires, respectively. The resulting particles were introduced into the smog chamber and exposed to UVA irradiation (λ = ~365 nm) after gas phase removal. With reactive gases excluded, SOA formation and its impact on OA oxidation were minimal.

Figure 1 presents the evolution in the BBOA composition as a function of jNO_2. The dashed lines represent the average of the time series observed from two dark ozonolysis experiments, considered as experimental control (i.e., same experimental conditions but without UVA light). Their experimental time is the same as the experimental time of photoinduced aging experiments, providing a basis for comparing the impact of chamber dilution and vapor wall losses, as the oxidation capacity of ozone toward BBOA is relatively limited.[40] With UVA irradiation only, the oxidation level of particles increased rapidly as a function of the photon exposure. CO_2^+, from more oxidized compounds, increased significantly with the atmospheric equivalent jNO_2 age. Conversely, $C_xH_y^+$ ion abundances, indicative of hydrocarbons and reduced species, decreased over time (Figure S2). Consistently, the O/C rose from 0.4 to 1.0 over an atmospheric equivalent jNO_2 age of 7 h, with a simultaneous decrease in the hydrogen-to-carbon (H/C) ratio. Comparatively, control experiments showed weak-to-no trends for the same parameters.

Among all fragment ions, $C_2H_4O_2^+$, a fragment characteristic of anhydrous sugars (e.g., levoglucosan) from cellulose burning, exhibited the fastest decay, becoming nearly undetectable after 7 h of photoaging. Simultaneous near-molecular measurements using an EES-TOF confirmed an even faster decline in anhydrous sugars, detected as $C_6H_{10}O_5Na^+$ adduct, suggesting that anhydrous sugar concentrations can be low even in lightly aged BBOA. This faster decay in $C_6H_{10}O_5Na^+$ likely reflects additional production of $C_2H_4O_2^+$ photoinduced aging. Control experiments showed a slower decrease in both ions, likely related to some losses in semivolatile vapors from dilution or vapor wall deposition. However, the rapid and substantial decay observed under UVA exposure indicates that photoinduced oxidation is the dominant process, and experimental artifacts have only a minor impact on interpretation.

In a subset of experiments, excessive methanol was added as an OH scavenger to mitigate any potential OH radicals generated in the chamber. During these test experiments, the results (Figure S2) remained consistent with those presented in Figure 1. Overall, the POA became more oxidized through photoinduced aging without OH oxidation and SOA formation.

A common approach to track OA aging is by visualizing AMS spectra in the f_{44}-f_{43} space. m/z 44 reflects highly oxidized compounds such as carboxylic acids and acyl peroxides,[41−43] while the $C_2H_3O^+$ ion at m/z 43 represents nonacid functional oxygenated groups such as saturated carbonyl groups.[44−46] In Figure 2, we compare the evolution of f_{44}-f_{43} during photo (UVA)-induced and OH-induced aging of BB emissions with ambient low-volatility OOA (LV-OOA) and semivolatile OOA (SV-OOA), observed in Zürich, Switzerland,[47] where seasonal changes in sources (BB in winter and biogenic in summer) affect OOA composition. Values of f_{43} and f_{44} in this study are consistent with reported fresh BBOA.[18,25,48,49] In the intraparticle photoaging experiments, f_{44} increased from ~0.04 to ~0.20 over 7 h of equivalent jNO_2 exposure, showing a clear shift from POA to LV-OOA. This suggests that photoinduced aging alone can rapidly transform BBOA into highly oxidized OA. Our findings align with recent studies showing that UV-irradiated BBOA drives the increase in aerosol f_{44},[28] and sulfate formation through multiphase SO_2 oxidation.[50] By extending the aging time scale, we demonstrate that intraparticle photochemistry can be a major contributor to LV-OOA formation in the early stage of BBOA aging, filling a key gap in our understanding of OA aging.

Downloaded from pubs.acs.org/esthag/article-pdf/60/34/24206/6704211/acs.est.6c02532.pdf by FORSCHUNGZENTRUM JUELICH user on 26 November 2026

https://doi.org/10.1021/acs.est.6c02532
Environ. Sci. Technol. 2026, 60, 24206−24216

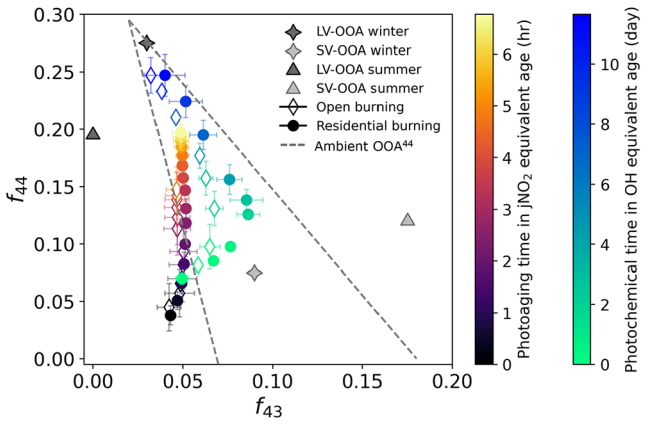

Figure 2. Scatter plot of f_{44} and f_{43} of OA from residential and open burning during aging processes by photoinduced aging of POA (without gas phase) with UVA light at a wavelength of 365 nm in jNO_2 equivalent age of hours and by OH oxidation of gas and aerosol phase of emissions in OH equivalent age of days. The error bars of markers represent the standard deviation from repeat experiments. To be consistent with source apportionment studies that lack high-resolution speciation, the mass fractions of ions at m/z 44 (f_{44}) and m/z 43 (f_{43}) were used instead of CO_2^+ and $C_2H_3O^+$, respectively. For the wood-burning experiments in this work, the vast majority of m/z 44 is due to the CO_2^+ fragment ion, as shown in Figure S4. This may not be the case in ambient measurements. The LV-OOA and SV-OOA denote low volatility and semivolatile oxygenated OA, which are source apportionment factors for Zürich.[47] These OOA factors show the oxidation level of OA, reflected by f_{44}, in the real atmosphere. In winter, OOA factors influenced by BB provide insight into the transition from SV-OOA to LV-OOA, serving as a reference for chamber experiments. The dashed line represents a range of ambient OOA.[44] The OH equivalent photochemical age is calculated by dividing the OH concentration in an oxidation flow reactor by the 24 h ambient typical average OH concentration, assuming 1.5×10^6 molecules cm^{-3} s^{-1}.[51]

Comparison of Photoinduced and Other Atmospheric Aging Processes

Figure 2 compares the effect of photoinduced and OH-driven aging on OA oxidation. OH oxidation experiments were performed by exposing BB gas and particle emissions to OH radicals in an OFR equipped with UVC lamps ($\lambda \approx 254$ nm). Although OH levels in some fire plumes can be higher than the typical ambient average,[38] they exhibit strong spatial and temporal variability. Therefore, OH exposure was converted into an atmospheric equivalent age using a typical 24-h average OH level (1.5×10^6 molecules cm^{-3}),[51] a commonly used reference that facilitates comparison across studies. As OH exposure increased, f_{43} initially rose, then declined, while f_{44} increased steadily (Figure 2). The initial increase in f_{43} reflects the formation of saturated carbonyl groups, such as alcohol, during the early stage of oxidation. With further oxidation, these alcohols are converted to more oxidized species such as carboxylic acids, leading to a decrease in f_{43} and an increase in f_{44}. However, it took 6−8 days of OH-equivalent aging to reach the oxidation levels comparable to those achieved after just 7 h of photoinduced aging. The O/C ratio increased from 0.5 to 1.2 over 8 days of OH-equivalent aging (Figure S5), consistent with previous chamber studies under lower OH concentrations.[52] These results highlight that photoinduced intraparticle oxidation at the early stage of BB oxidation is substantially faster than multigeneration OH-driven aging and may contribute to the high f_{44} levels observed in wintertime BBOA-influenced environments, such as in Zürich.

To confirm that only intraparticle photoinduced aging leads to such a rapid increase in OA oxidation, we performed three additional experiments:[1] OH oxidation of POA in the OFR, (2) ozonolysis of POA in the smog chamber, and (3) POA heating without any oxidants. In all cases, the gas phase species were removed using a charcoal denuder as in the photoinduced aging experiments. As shown in Figure S6 (with details in the SI), these processes led to minimal changes in oxidation state. Exposure of POA to OH in the OFR increased f_{44} by only 0.036 over 10 days of equivalent aging. UVC irradiation alone ($\lambda = 254$ nm) without OH generation in the OFR also showed no significant increase in f_{44}. Similarly, ozonolysis over 4 days of ozone-equivalent aging (based on an average ambient concentration of 40 ppb)[53] yielded a similar small increase in f_{44}. Heating POA to 150 °C in a thermodenuder, resulting in 85% mass loss, raised f_{44} by just 0.01. These results confirm that none of these alternative mechanisms can account for the substantial oxidation observed during intraparticle photoaging under UVA light.

Photoinduced Aging of BB Plumes in the Ambient Atmosphere

Airborne field measurements of BB plumes from wild and agricultural fires have frequently shown rapid oxidation of OA tracked through a steady increase in f_{44}, without a corresponding change in OA mass relative to CO, a long-lived BB emission.[17,19,20,54,55] In Figure 3, we revisit airborne observations in the aircraft measurements in FIREX-AQ and SAMBBA (see Methods Section) through the lens of our new laboratory findings to investigate whether photoinduced aging can account for the rapid OA oxidation observed in these plumes.

A bulk analysis of 210 crosswind transects of US wildfire plumes (FIREX-AQ) aged within 2 h was conducted, capturing how plume oxidation pathways vary across their structure by their tracer heterogeneity distribution. To track oxidation, we use the mass fraction of the CO_2^+ ion (fCO_2) instead of f_{44}, since large interfering fragments (such as $C_2H_4O^+$ and $C_2H_6N^+$) can contribute to m/z 44 signals in ambient plumes with high mass concentrations, which increase partitioning of semivolatile species to particles. Following the approach of Decker et al.,[37] we used the Gaussian Observational Model for Edge-to-Center Heterogeneity (GOMECH) to quantify how the spatial distribution of CO_2^+ differs from that of CO, which serves as a tracer for plume shape and dilution. A brief description of GOMECH can be found in the SI. Oxidation by OH can be inferred by gas-phase observations of maleic anhydride (MA), which is mostly formed by the OH oxidation of abundant furan species in BB emission.[56] As an OH chemistry proxy, MA has been shown to exhibit behavior similar to peroxyacetyl nitrate (PAN),[37] a well-known secondary photochemical pollutant. Although NO_3 oxidation can also contribute to furan oxidation and MA formation, results from FIREX-AQ indicate that furan compounds are oxidized predominantly by photochemical oxidation rather than NO_3.[57] Therefore, MA can be used as a tracer for OH-driven oxidation processes. Figure 3A compares the relationship between CO_2^+ and MA relative to CO for three plume categories based on emitted solar zenith angle (ESZA), a proxy for actinic flux, corresponding to midday (ESZA < 40°), afternoon (40°−60°), and evening (>60°) plumes. The

Downloaded from pubs.acs.org/esthag/article-pdf/60/34/24206/6704211/acs.est.6c02532.pdf by FORSCHUNGZENTRUM JUELICH user on 26 November 2026

https://doi.org/10.1021/acs.est.6c02532
Environ. Sci. Technol. 2026, 60, 24206−24216

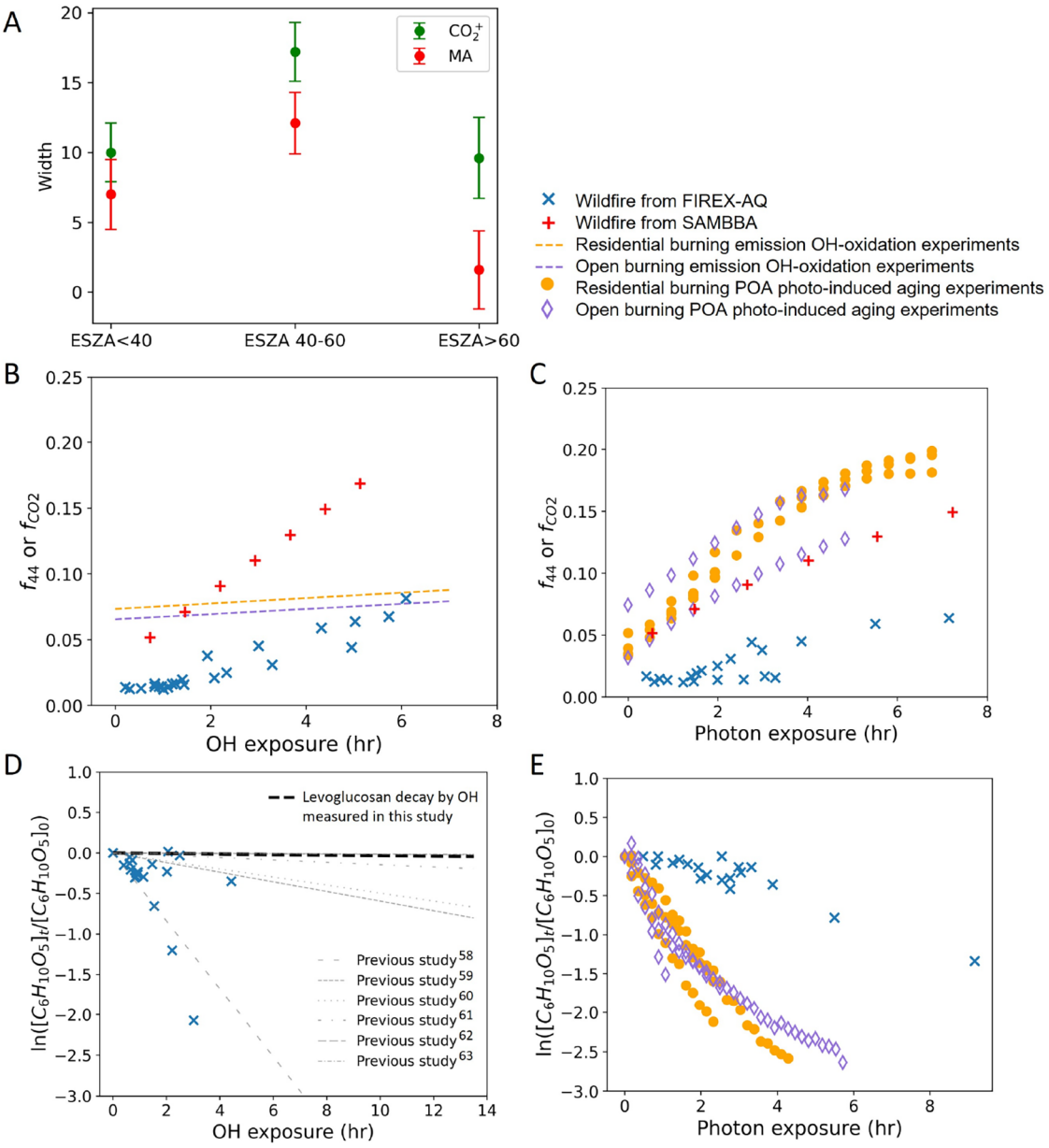

Figure 3. Comparison of chamber aging BBOA with aircraft measurement of BB plumes. (A) Plume width analysis using GOMECH fits on combined 210 crosswind wildfire transects from the NASA DC-8 aircraft, categorized based on the solar zenith angle at the time of emission (ESZA) into mid-day (ESZA < 40°), afternoon (40° < ESZA < 60°), and evening (ESZA > 60°). The error bars represent the uncertainty in the fit function in GOMECH with 90% confidence level. Both the CO_2^+ from AMS measurements, MA, and CO are normalized to a maximum of 1 for each plume (denoted by norm.). The CO_2^+ ion abundance is corrected for gaseous CO_2 contributions[66] and denoted as CO_2^+ (OA). Panel (B) compares the f_{44} during oxidation of gas and particle phase of BB emissions by OH in the OFR with f_{CO_2} observed from FIREX-AQ wildfires from 6 to 7 Aug. 2019 in the US and f_{44} from SAMBBA wildfires, 20 Sept. 2012 in Brazil. Panel (C) compares the same wildfire observations with the f_{44} during photoinduced aging of BB POA (without gas phase) with UVA light at a wavelength of 365 nm. Panel (D) shows the decay of $C_6H_{10}O_5$ (mainly levoglucosan) emitted from the wildfires on August 6th and 7th 2019, with OH exposure during FIREX-AQ. Levoglucosan abundance in FIREX-AQ is normalized by CO concentration to account for dilution effects. The black dashed line denotes the degradation of levoglucosan by OH oxidation, assuming an ambient 24 h OH concentration of 1.5×10^6 molecules cm^{-3} s^{-1} and the rate constant with the OH is 6.0×10^{-13} cm^3 $molecule^{-1}$ s^{-1}, derived from measurements in this study. The gray solid lines denote the degradation of levoglucosan by OH oxidation using rate constants from previous studies, also listed in Table S2. Panel (E) shows the decay of levoglucosan observed in photoinduced aging experiments with POA from three residential burning experiments and three open burning experiments, where EESI-TOF measurements are available, compared to field measurements in FIREX-AQ.

GOMECH fits reveal that both CO_2^+ and MA distributions are broader than CO in the afternoon, compared to midday and evening, indicating enhanced oxidation at plume edges, not explained by dilution alone, but consistent with the production of OOA species driven by sunlight exposure. Although oxidation via NO_3 radicals can occur in daytime biomass burning plumes,[57] NO_3 production is greatest in the plume core, and NO_3 oxidation products are more spatially confined than CO,[37] making this pathway unlikely to explain the observed edge-enhanced oxidation. More importantly, the

https://doi.org/10.1021/acs.est.6c02532
Environ. Sci. Technol. 2026, 60, 24206−24216

Downloaded from pubs.acs.org/esthag/article-pdf/60/34/24206/6704211/acs.est.6c02532.pdf by FORSCHUNGZENTRUM JUELICH user on 26 November 2026

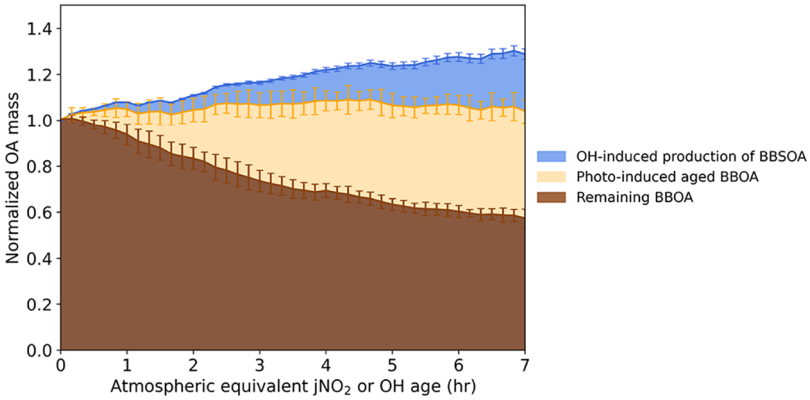

Figure 4. BBOA composition changes with the atmospheric equivalent time. The error bars denote the variation from repeat experiments. During photoinduced aging, ions measured by AMS having an increasing trend with irradiation are categorized as photoinduced aged BBOA; otherwise, it is the remaining BBOA. This gives the lower bound of photoinduced aged BBOA, as some reactant and product compounds could decompose to the same fragment ions in AMS. The OH-induced production of BB SOA is the exponential fitting of SOA production via OH oxidation in OFR (Figure S8). The change of BBOA composition caused by dilution-impacted processes (such as evaporation)[71] is not considered in these experiments.

greater plume width of CO_2^+ than MA, relative to CO, suggests that OH oxidation alone cannot explain the increased fCO_2. Instead, it points to additional photochemical aging occurring at the optically thinner edges of the plume.

Figure 3B shows the f_{44} as a function of OH equivalent age, while Figure 3C shows the f_{44} as a function of jNO_2 equivalent age. Both panels contain aircraft observations from FIREX-AQ and SAMBBA compared to laboratory measurements of OH- and photoinduced oxidation from this study. Panel B suggests that the values of f_{44} in POAs are different, yet the increase of f_{44} upon aging in the ambient plumes is generally greater than expected from only OH oxidation. The greater than expected oxidation in panel B is consistent with previous conclusions by field observations of smoke plumes,[15] indicating again that there must be other oxidation pathways driving the aging of BBOA in addition to OH chemistry. At the same time, panel C suggests that the oxidation level in the field observations is generally in good agreement (SAMBBA) or somewhat less (FIREX-AQ) than the expected aging by only photoinduced oxidation.

Given the complexity of chemical and physical processes in ambient plumes, we focus on levoglucosan, a tracer of BB emissions,[34,49] known to be relatively stable against OH. Figure 3D shows levoglucosan concentrations measured by EESI-TOF across three wildfire plume transects, plotted against estimated OH exposure. The reported rate constants for levoglucosan and OH from previous studies[58−63] span over three magnitudes due to particle-phase composition, viscosity, and experimental setup, as shown in Figure 3D and Table S2. Figure 3E compares ambient levoglucosan decay, plotted against total photon exposure between emission and sampling, with decay observed in our laboratory photoaging experiments. While the decay of levoglucosan in wildfire plumes correlates with both OH and UV exposure, it is significantly faster than OH oxidation alone derived from measurements in this study, as well as most previous estimates (Figure 3D), further excluding the contribution from OH oxidation and thus confirming that additional oxidation pathways contribute to the early stage BBOA aging in these plumes. While OH oxidation alone cannot account for the ambient degradation, the photoinduced aging pathway closes this gap (Figure 3E). Although levoglucosan is not photoreactive on its own, in mixtures with BBOA chromophores, it can contribute to a significant increase in the production of oxygen- and carbon-centered radicals under near-UV radiation, driving photochemical aging of BBOA in the atmosphere.[27] The decay of photosensitized levoglucosan in BBOA has also been recently observed in laboratory studies.[64] However, the laboratory-based photoaging in our study likely represents an upper limit for two reasons: (1) the UVA lamps used in the chamber have a narrower spectral range than natural sunlight; and (2) levoglucosan decay in the chamber was not corrected for vapor wall losses,[65] potentially exaggerating the apparent oxidation rate. These losses were estimated based on separate dark ozonolysis experiments used as a control (Figure S7), but differences in OA mass and particle size introduce uncertainties that prevent precise correction. Despite inherent limitations related to laboratory experiments, the rapid degradation of levoglucosan is observed in both the laboratory and the ambient atmosphere. Overall, radical-driven intraparticle photochemistry, rather than OH-induced SOA formation, is a key mechanism behind the rapid oxidation of BBOA and the production of OOA in biomass burning plumes.

Plausible Mechanistic Interpretation of Intraparticle Photochemistry

Intraparticle photochemistry proceeds an order of magnitude faster than oxidation with OH in the gas phase, currently considered the dominant atmospheric aging pathway. While the exact mechanism remains uncertain, laboratory experiments primarily based on surrogates of BBOA species suggest that radical-driven processes and autoxidation within the particle phase are most likely involved.

Brown carbon in BBOA absorbs UVA light, creating conditions favorable for photochemistry, where enhanced photon density within particles due to optical confinement can amplify reaction rates by up to a factor of 3.[67] Upon absorption, photosensitizing chromophores may generate OH radicals, singlet molecular oxygen ($^1O_2$), and triplet excited state organic matter ($^3C^*$),[26,27,50] potent oxidants in the particle phase. Recent studies have measured the quantum yields of $^1O_2$ and $^3C^*$ in fresh BBOA at 365 nm to be ∼2%, compared to ∼0.02% for OH.[68] Concentrations of $^3C^*$ can be 3−6 orders of magnitude higher than OH, and their reactivity

Downloaded from pubs.acs.org/esthag/article-pdf/60/34/24206/6704211/acs.est.6c02532.pdf by FORSCHUNGZENTRUM JUELICH user on 26 November 2026

https://doi.org/10.1021/acs.est.6c02532
Environ. Sci. Technol. 2026, 60, 24206−24216

toward phenolic compounds, which are abundant in biomass burning aerosols, can exceed OH autoxidation rates. $^1O_2$ and $^3C^*$ have been shown to produce larger molecular weight and more oxygenated compounds upon reactions.[26] By contrast, the degradation of compounds like levoglucosan observed here is evidence of intraparticle radical chemistry.

To assess photolytic aging kinetics, we summed BBOA ion signals that decreased under UVA exposure. As shown in Figure 4, over 7 h of ambient-equivalent actinic flux (jNO_2), BBOA mass declined by 43%, corresponding to a first-order photolysis rate of $2.2 \times 10^{-5} \pm 0.4 \times 10^{-5}$ s^{-1}. As part of these ions can also be produced through photochemistry, these estimates should be considered as lower bounds. The photolysis rate j can be expressed as $\int_{\lambda_1}^{\lambda_2} \sigma \cdot \Phi \cdot F d\lambda$, where σ is the absorption cross section, Φ is the quantum yield, and F is the actinic flux. $F\Delta\lambda$ can be constrained using the experimentally determined jNO_2 (2.9×10^3 s) and known σ and Φ values for NO_2 at 360 nm. Using the reported mass absorption efficiency (MAE) of BBOA of 1.37 m^2 g^{-1} at 370 nm[69], we estimate that the bulk value of Φ is 0.36% ± 0.13%, meaning that 0.36% of the absorbed light produces radicals that lead to oxidation. These yields, which can be used as direct inputs for chemical transport models to estimate fire plumes aging, are ten times higher than those reported for OH radicals, but ten times lower than those for $^1O_2$ and $^3C^*$.[68]

Contribution of Photoinduced Aging of BBOA to OOA in the Atmosphere

BB emits ∼36 Tg of POA annually, with contributions expected to rise further under climate change. Our findings call for a complete rethink of how biomass burning emissions age in the atmosphere. We show that this POA is highly reactive to sunlight, undergoing rapid transformation through photoinduced intraparticle radical chemistry. This mechanism generates OOA without invoking any gas-phase reactions. Within just 7 h of UVA exposure, 43% of primary BBOA is converted into OOA, nearly twice the contribution from gas-phase OH oxidation, which accounts for only 23% (Figure 4). While both fractions will be attributed to OOA in the atmosphere, our results reveal that early-stage aging is dominated by oxidized POA, challenging the long-standing view that OOA in biomass burning plumes is primarily driven by gas-phase chemistry.

This mechanism explains key ambient observations, including the rapid oxidation of BBOA observed in wildfire and prescribed burn plumes, as well as elevated O/C ratios seen in wintertime urban air influenced by residential burning.[13,47,70] Even under low winter UV levels, intraparticle photochemistry, proceeding roughly ten times faster than OH oxidation, plays a significant role during the first day of atmospheric aging. Beyond this timescale, traditional SOA formation is expected to dominate the OOA mass in biomass burning plumes. In regions with minimal biomass burning, OOA is likely still driven by the gas-phase oxidation of anthropogenic precursors. Our results also challenge the current source apportionment approaches. Tracers such as levoglucosan, commonly used to identify BBOA, degrade rapidly in the particle phase under sunlight, forming oxidized products without the involvement of gas-phase oxidants.

IMPLICATIONS

Beyond helping with the interpretation of long-standing field observations, our findings have important implications for both the climate and air quality. Rapid intraparticle photoinduced aging likely contributes to the formation of tarballs observed in wildfires within just a few hours and may drive continued aerosol darkening even after sunlight fades, sustained by long-lived reactive intermediates.[72] As oxidation progresses, it leads to more photorecalcitrant oxygenated compounds,[73] potentially altering aerosol hygroscopicity, atmospheric lifetimes, and interactions with clouds. Furthermore, the same reaction intermediates, including OH radicals, $^1O_2$, and $^3C^*$, are well-established reactive oxygen species (ROS) that trigger oxidative stress in human lungs. These results open new avenues for research into the broader climate and health impacts of aged biomass burning emissions.

While this study focused on BBOA from conifer wood burning, the core chemical composition of emissions from other biomass sources, such as straw and other types of wood, shares common features,[49] suggesting that the photoinduced aging mechanism is broadly applicable. Moreover, other OA fractions, particularly SOA containing aromatic oxidation products, also absorb light and may undergo similar photochemical transformations.

To deepen the mechanistic understanding, future work should include molecular-level characterization and spectroscopic analysis of aging BBOA and gas-phase compounds, the latter of which were not available in this study due to instrumental sensitivity limitations. Such efforts are essential to identify reactive intermediates, oxidation products, and their evolution over time.

Finally, our results highlight the need to reassess current atmospheric models, many of which underpredict the oxidation state of BBOAs. As wildfire frequency and intensity rise with climate change, incorporating photoinduced particle-phase aging into models is critical for improving projections of air quality, aerosol optical properties, and cloud interactions in a warming climate.

ASSOCIATED CONTENT

Supporting Information

The Supporting Information is available free of charge at https://pubs.acs.org/doi/10.1021/acs.est.6c02532.

Experimental information of photo-induced aging of BBOA; schematic diagram of experimental setup; the comparison of photo-induced aging experiments without and with methanol as the OH scavenger (PDF)

AUTHOR INFORMATION

Corresponding Authors

David M. Bell − *Laboratory of Atmospheric Chemistry, PSI Center for Energy and Environmental Sciences, Paul Scherrer Institute, Villigen 5232, Switzerland*; Email: david.bell@psi.ch

Imad El Haddad − *Laboratory of Atmospheric Chemistry, PSI Center for Energy and Environmental Sciences, Paul Scherrer Institute, Villigen 5232, Switzerland*; orcid.org/0000-0002-2461-7238; Email: imad.el-haddad@psi.ch

Andre S. H. Prevot − *Laboratory of Atmospheric Chemistry, PSI Center for Energy and Environmental Sciences, Paul Scherrer Institute, Villigen 5232, Switzerland*; orcid.org/0000-0002-9243-8194; Email: andre.prevot@psi.ch

Downloaded from pubs.acs.org/esthag/article-pdf/60/34/24206/6704211/acs.est.6c02532.pdf by FORSCHUNGZENTRUM JUELICH user on 26 November 2026

https://doi.org/10.1021/acs.est.6c02532
Environ. Sci. Technol. 2026, 60, 24206−24216

Authors

Jun Zhang − *Laboratory of Atmospheric Chemistry, PSI Center for Energy and Environmental Sciences, Paul Scherrer Institute, Villigen 5232, Switzerland;* orcid.org/0000-0002-6952-2785

Rico K. Y. Cheung − *Laboratory of Atmospheric Chemistry, PSI Center for Energy and Environmental Sciences, Paul Scherrer Institute, Villigen 5232, Switzerland*

Zachary C. J. Decker − *Laboratory of Atmospheric Chemistry, PSI Center for Energy and Environmental Sciences, Paul Scherrer Institute, Villigen 5232, Switzerland; Cooperative Institute for Research in Environmental Sciences (CIRES), University of Colorado, Boulder, Colorado 80309, United States; NOAA Chemical Sciences Laboratory (CSL), Boulder, Colorado 80305, United States*

Mihnea Surdu − *Laboratory of Atmospheric Chemistry, PSI Center for Energy and Environmental Sciences, Paul Scherrer Institute, Villigen 5232, Switzerland;* Present Address: Extreme Environments Research Laboratory, École Polytechnique Fédérale de Lausanne, Sion 1951, Switzerland; orcid.org/0000-0003-1815-2750

Sophie Bogler − *Institute of Environmental Engineering, Department of Civil, Environmental and Geomatic Engineering, ETH Zurich, Zurich 8093, Switzerland*

Kun Li − *Laboratory of Atmospheric Chemistry, PSI Center for Energy and Environmental Sciences, Paul Scherrer Institute, Villigen 5232, Switzerland;* Present Address: Environmental Research Institute, Shandong University, Qingdao 266237, China; orcid.org/0000-0003-2970-037X

Tiantian Wang − *Laboratory of Atmospheric Chemistry, PSI Center for Energy and Environmental Sciences, Paul Scherrer Institute, Villigen 5232, Switzerland*

Robin L. Modini − *Laboratory of Atmospheric Chemistry, PSI Center for Energy and Environmental Sciences, Paul Scherrer Institute, Villigen 5232, Switzerland;* orcid.org/0000-0002-2982-1369

Jay G. Slowik − *Laboratory of Atmospheric Chemistry, PSI Center for Energy and Environmental Sciences, Paul Scherrer Institute, Villigen 5232, Switzerland*

Demetrios Pagonis − *Department of Chemistry, University of Colorado Boulder, Boulder, Colorado 80309, United States; Cooperative Institute for Research in Environmental Sciences (CIRES), University of Colorado, Boulder, Colorado 80309, United States;* Present Address: Weber State University Department of Chemistry and Biochemistry, Ogden, Utah 84408, United States; orcid.org/0000-0002-0441-2614

Hongyu Guo − *Department of Chemistry, University of Colorado Boulder, Boulder, Colorado 80309, United States; Cooperative Institute for Research in Environmental Sciences (CIRES), University of Colorado, Boulder, Colorado 80309, United States;* orcid.org/0000-0003-0487-3610

Pedro Campuzano-Jost − *Department of Chemistry, University of Colorado Boulder, Boulder, Colorado 80309, United States; Cooperative Institute for Research in Environmental Sciences (CIRES), University of Colorado, Boulder, Colorado 80309, United States;* orcid.org/0000-0003-3930-010X

Jose L. Jimenez − *Cooperative Institute for Research in Environmental Sciences (CIRES), University of Colorado, Boulder, Colorado 80309, United States; NOAA Chemical Sciences Laboratory (CSL), Boulder, Colorado 80305, United States;* orcid.org/0000-0001-6203-1847

Matthew M. Coggon − *NOAA Chemical Sciences Laboratory (CSL), Boulder, Colorado 80305, United States;* orcid.org/0000-0002-5763-1925

Georgios I. Gkatzelis − *Cooperative Institute for Research in Environmental Sciences (CIRES), University of Colorado, Boulder, Colorado 80309, United States; NOAA Chemical Sciences Laboratory (CSL), Boulder, Colorado 80305, United States;* Present Address: Institute of Climate and Energy Systems, ICE-3: Troposphere, Forschungszentrum Jülich GmbH, Jülich 52425, Germany; orcid.org/0000-0002-4608-3695

Carsten Warneke − *NOAA Chemical Sciences Laboratory (CSL), Boulder, Colorado 80305, United States;* orcid.org/0000-0003-3811-8496

Samuel R. Hall − *Atmospheric Chemistry Observations and Modeling Laboratory, National Center for Atmospheric Research, Boulder, Colorado 80301, United States*

Kirk Ullmann − *Atmospheric Chemistry Observations and Modeling Laboratory, National Center for Atmospheric Research, Boulder, Colorado 80301, United States*

Glenn S. Diskin − *NASA Langley Research Center, Hampton, Virginia 23681, United States;* orcid.org/0000-0002-3617-0269

Joshua P. Digangi − *NASA Langley Research Center, Hampton, Virginia 23681, United States;* orcid.org/0000-0002-6764-8624

Jeff Peischl − *Cooperative Institute for Research in Environmental Sciences (CIRES), University of Colorado, Boulder, Colorado 80309, United States; NOAA Chemical Sciences Laboratory (CSL), Boulder, Colorado 80305, United States;* orcid.org/0000-0002-9320-7101

Christopher D. Holmes − *Department of Earth, Ocean, and Atmospheric Science, Florida State University, Tallahassee, Florida 32304, United States;* orcid.org/0000-0002-2727-0954

Shan Zhou − *Department of Environmental Toxicology, University of California, Davis, California 95616, United States;* Present Address: School of Environmental and Sustainable Engineering, Eastern Institute of Technology, Ningbo 315000, China

Qi Zhang − *Department of Environmental Toxicology, University of California, Davis, California 95616, United States;* orcid.org/0000-0002-5203-8778

Complete contact information is available at: https://pubs.acs.org/10.1021/acs.est.6c02532

Author Contributions

J.Z., R.K.Y., and T.T.W. conducted the photoinduced aging experiments. J.Z. and K.L. conducted SOA formation experiments. S.B. and R.K.Y. conducted the ozonolysis experiment. J.Z. and D.M.B. conducted the evaporation experiment. M.S. conducted the levoglucosan measurement for the chamber experiments. Z.C.J.D. analyzed the FIREX-AQ data and assisted in the preparation of figures. The FIREX-AQ relevant data is provided by D.P., H.G., P.C.J., and J.L.J. (f_{CO_2}, m/z 44, OA, levoglucosan), M.M.C., G.I.G., and C.W. (VOCs), S.R.H. and K.U. (actinic flux), G.S.D., J.P., and J.P.D. (CO), and C.D.H. (plume age). J.Z. prepared the preliminary manuscript with contributions from all coauthors. I.E.H. revised and modified the manuscript. R.L.M., D.M.B., I.E.H., and A.S.H.P. led the project and data interpretation.

Downloaded from pubs.acs.org/esthag/article-pdf/60/34/24206/6704211/acs.est.6c02532.pdf by FORSCHUNGZENTRUM JUELICH user on 26 November 2026

https://doi.org/10.1021/acs.est.6c02532
Environ. Sci. Technol. 2026, 60, 24206−24216

Notes

The authors declare no competing financial interest.

■ ACKNOWLEDGMENTS

We thank the financial support from the Swiss National Science Foundation (MOLORG grant 200020_188624 and Sino-Swiss Joint Research Project IZLCZ0_189883). PSI's atmospheric simulation chamber is a facility of the ACTRIS ERIC and receives funding from the Swiss State Secretariat for Education, Research and Innovation (SERI grant). D.P., H.G., P.C.J., and J.L.J. acknowledge NASA Support through Grants 80NSSC18K0630, 80NSSC21K1451, and 80NSSC23K0828, and NSF AGS 2206655. S.H. and K.U. are supported by the NSF National Center for Atmospheric Research, which is a major facility sponsored by the U.S. National Science Foundation under Cooperative Agreement No. 1852977. Their research was funded by NASA Award No. 80NSSC18K0638. C.D.H. was supported by a NASA grant 80NSSC18K0625. J.P. acknowledges NOAA cooperative agreements NA17OAR4320101 and NA22OAR4320151.

■ REFERENCES

(1) Andreae, M. O. Emission of trace gases and aerosols from biomass burning − an updated assessment. *Atmos. Chem. Phys.* **2019**, *19* (13), 8523−8546.

(2) Karanasiou, A.; Alastuey, A.; Amato, F.; Renzi, M.; Stafoggia, M.; Tobias, A.; Reche, C.; Forastiere, F.; Gumy, S.; Mudu, P.; Querol, X. Short-term health effects from outdoor exposure to biomass burning emissions: A review. *Sci. Total Environ.* **2021**, *781*, No. 146739.

(3) Liu, L.; Cheng, Y.; Wang, S.; Wei, C.; Pöhlker, M. L.; Pöhlker, C.; Artaxo, P.; Shrivastava, M.; Andreae, M. O.; Pöschl, U.; Su, H. Impact of biomass burning aerosols on radiation, clouds, and precipitation over the Amazon: relative importance of aerosol−cloud and aerosol−radiation interactions. *Atmos. Chem. Phys.* **2020**, *20* (21), 13283−13301.

(4) Mansoor, S.; Farooq, I.; Kachroo, M. M.; Mahmoud, A. E. D.; Fawzy, M.; Popescu, S. M.; Alyemeni, M. N.; Sonne, C.; Rinklebe, J.; Ahmad, P. Elevation in wildfire frequencies with respect to the climate change. *J. Environ. Manage.* **2022**, *301*, No. 113769.

(5) Westerling, A. L.; Hidalgo, H. G.; Cayan, D. R.; Swetnam, T. W. Warming and Earlier Spring Increase Western U.S. Forest Wildfire Activity. *Science* **2006**, *313*, 940−943.

(6) Pagonis, D.; Selimovic, V.; Campuzano-Jost, P.; Guo, H.; Day, D. A.; Schueneman, M. K.; Nault, B. A.; Coggon, M. M.; DiGangi, J. P.; Diskin, G. S.; et al. Impact of Biomass Burning Organic Aerosol Volatility on Smoke Concentrations Downwind of Fires. *Environ. Sci. Technol.* **2023**, *57* (44), 17011−17021.

(7) Li, K.; Zhang, J.; Bell, D. M.; Wang, T.; Lamkaddam, H.; Cui, T.; Qi, L.; Surdu, M.; Wang, D.; Du, L.; et al. Uncovering the dominant contribution of intermediate volatility compounds in secondary organic aerosol formation from biomass-burning emissions. *Natl. Sci. Rev.* **2024**, *11*, No. nwae014.

(8) Slade, J. H.; Knopf, D. A. Heterogeneous OH oxidation of biomass burning organic aerosol surrogate compounds: assessment of volatilisation products and the role of OH concentration on the reactive uptake kinetics. *Phys. Chem. Chem. Phys.* **2013**, *15* (16), 5898−5915.

(9) Canagaratna, M. R.; Jimenez, J. L.; Kroll, J. H.; Chen, Q.; Kessler, S. H.; Massoli, P.; Hildebrandt Ruiz, L.; Fortner, E.; Williams, L. R.; Wilson, K. R.; et al. Elemental ratio measurements of organic compounds using aerosol mass spectrometry: characterization, improved calibration, and implications. *Atmos. Chem. Phys.* **2015**, *15* (1), 253−272.

(10) Canonaco, F.; Tobler, A.; Chen, G.; Sosedova, Y.; Slowik, J. G.; Bozzetti, C.; Daellenbach, K. R.; El Haddad, I.; Crippa, M.; Huang, R. J.; et al. A new method for long-term source apportionment with time-dependent factor profiles and uncertainty assessment using SoFi Pro: application to 1 year of organic aerosol data. *Atmos. Meas. Technol.* **2021**, *14* (2), 923−943.

(11) Crippa, M.; Canonaco, F.; Lanz, V. A.; Äijälä, M.; Allan, J. D.; Carbone, S.; Capes, G.; Ceburnis, D.; Dall'Osto, M.; Day, D. A.; et al. Organic aerosol components derived from 25 AMS data sets across Europe using a consistent ME-2 based source apportionment approach. *Atmos. Chem. Phys.* **2014**, *14* (12), 6159−6176.

(12) Schroder, J. C.; Campuzano-Jost, P.; Day, D. A.; Shah, V.; Larson, K.; Sommers, J. M.; Sullivan, A. P.; Campos, T.; Reeves, J. M.; Hills, A.; et al. Sources and Secondary Production of Organic Aerosols in the Northeastern United States during WINTER. *J. Geophys. Res.: Atmos.* **2018**, *123* (14), 7771−7796.

(13) Chen, G.; Canonaco, F.; Tobler, A.; Aas, W.; Alastuey, A.; Allan, J.; Atabakhsh, S.; Aurela, M.; Baltensperger, U.; Bougiatioti, A.; et al. European aerosol phenomenology − 8: Harmonised source apportionment of organic aerosol using 22 Year-long ACSM/AMS datasets. *Environ. Int.* **2022**, *166*, No. 107325.

(14) Qi, L.; Chen, M.; Stefenelli, G.; Pospisilova, V.; Tong, Y.; Bertrand, A.; Hueglin, C.; Ge, X.; Baltensperger, U.; Prévôt, A. S. H.; Slowik, J. G. Organic aerosol source apportionment in Zurich using an extractive electrospray ionization time-of-flight mass spectrometer (EESI-TOF-MS) − Part 2: Biomass burning influences in winter. *Atmos. Chem. Phys.* **2019**, *19* (12), 8037−8062.

(15) Hodshire, A. L.; Akherati, A.; Alvarado, M. J.; Brown-Steiner, B.; Jathar, S. H.; Jimenez, J. L.; Kreidenweis, S. M.; Lonsdale, C. R.; Onasch, T. B.; Ortega, A. M.; Pierce, J. R. Aging Effects on Biomass Burning Aerosol Mass and Composition: A Critical Review of Field and Laboratory Studies. *Environ. Sci. Technol.* **2019**, *53* (17), 10007−10022.

(16) Jolleys, M. D.; Coe, H.; McFiggans, G.; Capes, G.; Allan, J. D.; Crosier, J.; Williams, P. I.; Allen, G.; Bower, K. N.; Jimenez, J. L.; et al. Characterizing the aging of biomass burning organic aerosol by use of mixing ratios: a meta-analysis of four regions. *Environ. Sci. Technol.* **2012**, *46* (24), 13093−13102.

(17) Cubison, M. J.; Ortega, A. M.; Hayes, P. L.; Farmer, D. K.; Day, D.; Lechner, M. J.; Brune, W. H.; Apel, E.; Diskin, G. S.; Fisher, J. A.; et al. Effects of aging on organic aerosol from open biomass burning smoke in aircraft and laboratory studies. *Atmos. Chem. Phys.* **2011**, *11* (23), 12049−12064.

(18) Morgan, W. T.; Allan, J. D.; Bauguitte, S.; Darbyshire, E.; Flynn, M. J.; Lee, J.; Liu, D.; Johnson, B.; Haywood, J.; Longo, K. M.; et al. Transformation and ageing of biomass burning carbonaceous aerosol over tropical South America from aircraft in situ measurements during SAMBBA. *Atmos. Chem. Phys.* **2020**, *20* (9), 5309−5326.

(19) Garofalo, L. A.; Pothier, M. A.; Levin, E. J. T.; Campos, T.; Kreidenweis, S. M.; Farmer, D. K. Emission and Evolution of Submicron Organic Aerosol in Smoke from Wildfires in the Western United States. *ACS Earth Space Chem.* **2019**, *3* (7), 1237−1247.

(20) Liu, X.; Zhang, Y.; Huey, L. G.; Yokelson, R. J.; Wang, Y.; Jimenez, J. L.; Campuzano-Jost, P.; Beyersdorf, A. J.; Blake, D. R.; Choi, Y.; et al. Agricultural fires in the southeastern U.S. during SEACRS: Emissions of trace gases and particles and evolution of ozone, reactive nitrogen, and organic aerosol. *J. Geophys. Res.: Atmos.* **2016**, *121* (12), 7383−7414.

(21) Xiao, M.; Wang, M.; Mentler, B.; Garmash, O.; Lamkaddam, H.; Molteni, U.; Simon, M.; Ahonen, L.; Amorim, A.; Baccarini, A.; et al. Anthropogenic organic aerosol in Europe produced mainly through second-generation oxidation. *Nat. Geosci.* **2025**, *18* (3), 239−245.

(22) Lim, C. Y.; Hagan, D. H.; Coggon, M. M.; Koss, A. R.; Sekimoto, K.; de Gouw, J.; Warneke, C.; Cappa, C. D.; Kroll, J. H. Secondary organic aerosol formation from the laboratory oxidation of biomass burning emissions. *Atmos. Chem. Phys.* **2019**, *19* (19), 12797−12809.

(23) Ahern, A. T.; Robinson, E. S.; Tkacik, D. S.; Saleh, R.; Hatch, L. E.; Barsanti, K. C.; Stockwell, C. E.; Yokelson, R. J.; Presto, A. A.; Robinson, A. L.; et al. Production of Secondary Organic Aerosol

Downloaded from pubs.acs.org/esthag/article-pdf/60/34/24206/6704211/acs.est.6c02532.pdf by FORSCHUNGZENTRUM JUELICH user on 26 November 2026

https://doi.org/10.1021/acs.est.6c02532
Environ. Sci. Technol. 2026, 60, 24206−24216

During Aging of Biomass Burning Smoke From Fresh Fuels and Its Relationship to VOC Precursors. *J. Geophys. Res.: Atmos.* **2019**, *124* (6), 3583−3606.
(24) Bertrand, A.; Stefenelli, G.; Bruns, E. A.; Pieber, S. M.; Temime-Roussel, B.; Slowik, J. G.; Prévôt, A. S. H.; Wortham, H.; El Haddad, I.; Marchand, N. Primary emissions and secondary aerosol production potential from woodstoves for residential heating: Influence of the stove technology and combustion efficiency. *Atmos. Environ.* **2017**, *169*, 65−79.
(25) Fang, Z.; Deng, W.; Zhang, Y.; Ding, X.; Tang, M.; Liu, T.; Hu, Q.; Zhu, M.; Wang, Z.; Yang, W.; et al. Open burning of rice, corn and wheat straws: primary emissions, photochemical aging, and secondary organic aerosol formation. *Atmos. Chem. Phys.* **2017**, *17* (24), 14821−14839.
(26) Liu-Kang, C.; Sokolova, A.; Gong, Y.; Fahy, W. D.; Peng, H.; Abbatt, J. P. D. Light Exposure of Wood Smoke Aerosol: Connecting Optical Properties, Oxidation, Radical Formation, and Chemical Composition. *ACS EST Air* **2024**, *1* (4), 273−282.
(27) Gerritz, L.; Schervish, M.; Lakey, P. S. J.; Oeij, T.; Wei, J.; Nizkorodov, S. A.; Shiraiwa, M. Photoenhanced Radical Formation in Aqueous Mixtures of Levoglucosan and Benzoquinone: Implications to Photochemical Aging of Biomass-Burning Organic Aerosols. *J. Phys. Chem. A* **2023**, *127* (24), 5209−5221.
(28) Liu-Kang, C.; Gallimore, P. J.; Liu, T.; Abbatt, J. P. D. Photoreaction of biomass burning brown carbon aerosol particles. *Environ. Sci.: Atmos.* **2022**, *2* (2), 270−278.
(29) Liu-Kang, C.; Rivellini, L.-H.; Wang, X.; Abbatt, J. P. D. Rapid Nighttime Darkening of Biomass Burning Brown Carbon by Nitrate Radicals Is Suppressed by Prior Daytime Photochemical Aging. *ACS Earth Space Chem.* **2025**, *9*, 1124−1133.
(30) Lee, C. P.; Surdu, M.; Bell, D. M.; Lamkaddam, H.; Wang, M.; Ataei, F.; Hofbauer, V.; Lopez, B.; Donahue, N. M.; Dommen, J.; et al. Effects of aerosol size and coating thickness on the molecular detection using extractive electrospray ionization. *Atmos. Meas. Technol.* **2021**, *14* (9), 5913−5923.
(31) Hodzic, A.; Madronich, S.; Kasibhatla, P. S.; Tyndall, G.; Aumont, B.; Jimenez, J. L.; Lee-Taylor, J.; Orlando, J. Organic photolysis reactions in tropospheric aerosols: effect on secondary organic aerosol formation and lifetime. *Atmos. Chem. Phys.* **2015**, *15* (16), 9253−9269.
(32) Li, K.; Liggio, J.; Lee, P.; Han, C.; Liu, Q.; Li, S.-M. Secondary organic aerosol formation from α-pinene, alkanes, and oil-sands-related precursors in a new oxidation flow reactor. *Atmos. Chem. Phys.* **2019**, *19* (15), 9715−9731.
(33) Lopez-Hilfiker, F. D.; Pospisilova, V.; Huang, W.; Kalberer, M.; Mohr, C.; Stefenelli, G.; Thornton, J. A.; Baltensperger, U.; Prevot, A. S. H.; Slowik, J. G. An extractive electrospray ionization time-of-flight mass spectrometer (EESI-TOF) for online measurement of atmospheric aerosol particles. *Atmos. Meas. Technol.* **2019**, *12* (9), 4867−4886.
(34) Zhang, J.; Zuend, A.; Top, J.; Surdu, M.; Ei Haddad, I.; Slowik, J. G.; Prevot, A. S. H.; Bell, D. M. Estimation of the Volatility and Apparent Activity Coefficient of Levoglucosan in Wood-Burning Organic Aerosols. *Environ. Sci. Technol. Lett.* **2024**, *11* (11), 1214−1219.
(35) DeCarlo, P. F.; Kimmel, J. R.; Trimborn, A.; Northway, M. J.; Jayne, J. T.; Aiken, A. C.; Gonin, M.; Fuhrer, K.; Horvath, T.; Docherty, K. S.; et al. Field-Deployable, High-Resolution, Time-of-Flight Aerosol Mass Spectrometer. *Anal. Chem.* **2006**, *78* (24), 8281−8289.
(36) Warneke, C.; Schwarz, J. P.; Dibb, J.; Kalashnikova, O.; Frost, G.; Al-Saad, J.; Brown, S. S.; Brewer, W. A.; Soja, A.; Seidel, F. C.; et al. Fire Influence on Regional to Global Environments and Air Quality (FIREX-AQ). *J. Geophys. Res.: Atmos.* **2023**, *128* (2), No. e2022JD037758.
(37) Decker, Z. C. J.; Wang, S.; Bourgeois, I.; Campuzano Jost, P.; Coggon, M. M.; DiGangi, J. P.; Diskin, G. S.; Flocke, F. M.; Franchin, A.; Fredrickson, C. D.; et al. Novel Analysis to Quantify Plume Crosswind Heterogeneity Applied to Biomass Burning Smoke. *Environ. Sci. Technol.* **2021**, *55* (23), 15646−15657.
(38) Xu, L.; Crounse, J. D.; Vasquez, K. T.; Allen, H.; Wennberg, P. O.; Bourgeois, I.; Brown, S. S.; Campuzano-Jost, P.; Coggon, M. M.; Crawford, J. H.; et al. Ozone chemistry in western U.S. wildfire plumes. *Sci. Adv.* **2021**, *7* (50), No. eabl3648.
(39) Ringsdorf, A.; Edtbauer, A.; de Arellano, J. V.-G.; Pfannerstill, E. Y.; Gromov, S.; Kumar, V.; Pozzer, A.; Wolff, S.; Tsokankunku, A.; Soergel, M.; et al. Inferring the diurnal variability of OH radical concentrations over the Amazon from BVOC measurements. *Sci. Rep.* **2023**, *13* (1), No. 14900.
(40) Bogler, S.; Zhang, J.; Cheung, R. K. Y.; Li, K.; Prevot, A. S. H.; El Haddad, I.; Bell, D. M. Ozonolysis of primary biomass burning organic aerosol particles: Insights into reactivity and phase state. *Atmos. Chem. Phys.* **2025**, *25*, 10229−10243.
(41) Aiken, A. C.; DeCarlo, P. F.; Jimenez, J. L. Elemental Analysis of Organic Species with Electron Ionization High-Resolution Mass Spectrometry. *Anal. Chem.* **2007**, *79* (21), 8350−8358.
(42) Takegawa, N.; Miyakawa, T.; Kawamura, K.; Kondo, Y. Contribution of Selected Dicarboxylic and ω-Oxocarboxylic Acids in Ambient Aerosol to the m/z 44 Signal of an Aerodyne Aerosol Mass Spectrometer. *Aerosol Sci. Technol.* **2007**, *41* (4), 418−437.
(43) Yatavelli, R. L. N.; Mohr, C.; Stark, H.; Day, D. A.; Thompson, S. L.; Lopez-Hilfiker, F. D.; Campuzano-Jost, P.; Palm, B. B.; Vogel, A. L.; Hoffmann, T.; et al. Estimating the contribution of organic acids to northern hemispheric continental organic aerosol. *Geophys. Res. Lett.* **2015**, *42* (14), 6084−6090.
(44) Ng, N. L.; Canagaratna, M. R.; Zhang, Q.; Jimenez, J. L.; Tian, J.; Ulbrich, I. M.; Kroll, J. H.; Docherty, K. S.; Chhabra, P. S.; Bahreini, R.; et al. Organic aerosol components observed in Northern Hemispheric datasets from Aerosol Mass Spectrometry. *Atmos. Chem. Phys.* **2010**, *10* (10), 4625−4641.
(45) Yazdani, A.; Dudani, N.; Takahama, S.; Bertrand, A.; Prévôt, A. S. H.; El Haddad, I.; Dillner, A. M.Fragment ion-functional group relationships in organic aerosols using aerosol mass spectrometry and mid-infrared spectroscopy. In *Atmospheric Measurement Techniques*; Copernicus Publications, 2021 .
(46) Yazdani, A.; Dudani, N.; Takahama, S.; Bertrand, A.; Prévôt, A. S. H.; El Haddad, I.; Dillner, A. M. Characterization of primary and aged wood burning and coal combustion organic aerosols in an environmental chamber and its implications for atmospheric aerosols. *Atmos. Chem. Phys.* **2021**, *21* (13), 10273−10293.
(47) Canonaco, F.; Slowik, J. G.; Baltensperger, U.; Prévôt, A. S. H. Seasonal differences in oxygenated organic aerosol composition: implications for emissions sources and factor analysis. *Atmos. Chem. Phys.* **2015**, *15* (12), 6993−7002.
(48) Hennigan, C. J.; Miracolo, M. A.; Engelhart, G. J.; May, A. A.; Presto, A. A.; Lee, T.; Sullivan, A. P.; McMeeking, G. R.; Coe, H.; Wold, C. E.; et al. Chemical and physical transformations of organic aerosol from the photo-oxidation of open biomass burning emissions in an environmental chamber. *Atmos. Chem. Phys.* **2011**, *11* (15), 7669−7686.
(49) Zhang, J.; Li, K.; Wang, T.; Gammelsæter, E.; Cheung, R. K. Y.; Surdu, M.; Bogler, S.; Bhattu, D.; Wang, D. S.; Cui, T.; et al. Bulk and molecular-level composition of primary organic aerosol from wood, straw, cow dung, and plastic burning. *Atmos. Chem. Phys.* **2023**, *23* (22), 14561−14576.
(50) Liang, Z.; Zhou, L.; Chang, Y.; Qin, Y.; Chan, C. K. Biomass-burning organic aerosols as a pool of atmospheric reactive triplets to drive multiphase sulfate formation. *Proc. Natl. Acad. Sci. U.S.A.* **2024**, *121* (51), No. e2416803121.
(51) Mao, J.; Ren, X.; Brune, W. H.; Olson, J. R.; Crawford, J. H.; Fried, A.; Huey, L. G.; Cohen, R. C.; Heikes, B.; Singh, H. B.; et al. Airborne measurement of OH reactivity during INTEX-B. *Atmos. Chem. Phys.* **2009**, *9* (1), 163−173.
(52) Lim, C. Y.; Hagan, D. H.; Coggon, M. M.; Koss, A. R.; Sekimoto, K.; de Gouw, J.; Warneke, C.; Cappa, C. D.; Kroll, J. H. Secondary organic aerosol formation from the laboratory oxidation of

Downloaded from pubs.acs.org/esthag/article-pdf/60/34/24206/6704211/acs.est.6c02532.pdf by FORSCHUNGZENTRUM JUELICH user on 26 November 2026

https://doi.org/10.1021/acs.est.6c02532
Environ. Sci. Technol. 2026, 60, 24206−24216

biomass burning emissions. *Atmos. Chem. Phys.* **2019**, *19* (19), 12797−12809.
(53) World Meteorological Organization. Highlights from the Global Atmosphere Watch Programme. 2018; Vol. 2, p 8.
(54) Wu, H.; Taylor, J. W.; Langridge, J. M.; Yu, C.; Allan, J. D.; Szpek, K.; Cotterell, M. I.; Williams, P. I.; Flynn, M.; Barker, P.; et al. Rapid transformation of ambient absorbing aerosols from West African biomass burning. *Atmos. Chem. Phys.* **2021**, *21* (12), 9417−9440.
(55) Forrister, H.; Liu, J.; Scheuer, E.; Dibb, J.; Ziemba, L.; Thornhill, K. L.; Anderson, B.; Diskin, G.; Perring, A. E.; Schwarz, J. P.; et al. Evolution of brown carbon in wildfire plumes. *Geophys. Res. Lett.* **2015**, *42* (11), 4623−4630.
(56) Romanias, M. N.; Coggon, M. M.; Al Ali, F.; Burkholder, J. B.; Dagaut, P.; Decker, Z.; Warneke, C.; Stockwell, C. E.; Roberts, J. M.; Tomas, A.; et al. Emissions and Atmospheric Chemistry of Furanoids from Biomass Burning: Insights from Laboratory to Atmospheric Observations. *ACS Earth Space Chem.* **2024**, *8* (5), 857−899.
(57) Decker, Z. C. J.; Robinson, M. A.; Barsanti, K. C.; Bourgeois, I.; Coggon, M. M.; DiGangi, J. P.; Diskin, G. S.; Flocke, F. M.; Franchin, A.; Fredrickson, C. D.; et al. Nighttime and daytime dark oxidation chemistry in wildfire plumes: an observation and model analysis of FIREX-AQ aircraft data. *Atmos. Chem. Phys.* **2021**, *21* (21), 16293−16317.
(58) Zhang, W.; Xu, L.; Thadiyampurath, S.; Liu, X.; Leong, T.; Pagonis, D.; Campuzano-Jost, P.; Jimenez, J.; Robinson, M.; Veres, P.; DiGangi, J.; Halliday, H.; Nowak, J.; Diskin, G.; Zhang, H. Rapid Levoglucosan Oxidation as a Key Process in Biomass Burning Aerosol Aging. *Environ. Sci. Technol.* **2026**, *60* (1), 983−995.
(59) Hennigan, C. J.; Sullivan, A. P.; Collett, J. L.; Robinson, A. L.Levoglucosan stability in biomass burning particles exposed to hydroxyl radicals *Geophys. Res. Lett.* 2010; Vol. *37* 9.
(60) Lai, C.; Liu, Y.; Ma, J.; Ma, Q.; He, H. Degradation kinetics of levoglucosan initiated by hydroxyl radical under different environmental conditions. *Atmos. Environ.* **2014**, *91*, 32−39.
(61) Sang, X. F.; Gensch, I.; Kammer, B.; Khan, A.; Kleist, E.; Laumer, W.; Schlag, P.; Schmitte, S. H.; Wildt, J.; Zhao, R.; Mungall, E. L.; Abbatt, J. P. D.; Kiendler-Scharr. Chemical stability of levoglucosan: An isotopic perspective. *Geophys. Res. Lett.* **2016**, *43* (10), 5419−5424.
(62) Kessler, S. H.; Smith, J. D.; Che, D. L.; Worsnop, D. R.; Wilson, K. R.; Kroll, J. H. Chemical Sinks of Organic Aerosol: Kinetics and Products of the Heterogeneous Oxidation of Erythritol and Levoglucosan. *Environ. Sci. Technol.* **2010**, *44* (18), 7005−7010.
(63) Bai, J.; Sun, X.; Zhang, C.; Xu, Y.; Qi, C. The OH-initiated atmospheric reaction mechanism and kinetics for levoglucosan emitted in biomass burning. *Chemosphere* **2013**, *93* (9), 2004−2010.
(64) Liang, Z.; Liyuan, Z.; ChakK, C. Photosensitized Decay of Levoglucosan in Biomass Burning Aerosol Particles. *Environ. Sci. Technol.* **2025**, *59* (35), 18749−18760.
(65) Bertrand, A.; Stefenelli, G.; Pieber, S. M.; Bruns, E. A.; Temime-Roussel, B.; Slowik, J. G.; Wortham, H.; Prévôt, A. S. H.; El Haddad, I.; Marchand, N. Influence of the vapor wall loss on the degradation rate constants in chamber experiments of levoglucosan and other biomass burning markers. *Atmos. Chem. Phys.* **2018**, *18* (15), 10915−10930.
(66) Collier, S.; Zhang, Q. Gas-Phase CO2 Subtraction for Improved Measurements of the Organic Aerosol Mass Concentration and Oxidation Degree by an Aerosol Mass Spectrometer. *Environ. Sci. Technol.* **2013**, *47* (24), 14324−14331.
(67) Arroyo, P. C.; David, G.; Alpert, P. A.; Parmentier, E. A.; Ammann, M.; Signorell, R. Amplification of light within aerosol particles accelerates in-particle photochemistry. *Science* **2022**, *376* (6590), 293−296.
(68) Ma, L.; Worland, R.; Heinlein, L.; Guzman, C.; Jiang, W.; Niedek, C.; Bein, K. J.; Zhang, Q.; Anastasio, C. Seasonal variations in photooxidant formation and light absorption in aqueous extracts of ambient particles. *Atmos. Chem. Phys.* **2024**, *24* (1), 1−21.
(69) Moschos, V.; Kumar, N. K.; Daellenbach, K. R.; Baltensperger, U.; Prévôt, A. S. H.; El Haddad, I. Source Apportionment of Brown Carbon Absorption by Coupling Ultraviolet-Visible Spectroscopy with Aerosol Mass Spectrometry. *Environ. Sci. Technol. Lett.* **2018**, *5* (6), 302−308.
(70) Qi, L.; Vogel, A. L.; Esmaeilirad, S.; Cao, L.; Zheng, J.; Jaffrezo, J.-L.; Fermo, P.; Kasper-Giebl, A.; Daellenbach, K. R.; Chen, M.; et al. A 1-year characterization of organic aerosol composition and sources using an extractive electrospray ionization time-of-flight mass spectrometer (EESI-TOF). *Atmos. Chem. Phys.* **2020**, *20* (13), 7875−7893.
(71) June, N. A.; Hodshire, A. L.; Wiggins, E. B.; Winstead, E. L.; Robinson, C. E.; Thornhill, K. L.; Sanchez, K. J.; Moore, R. H.; Pagonis, D.; Guo, H.; et al. Aerosol size distribution changes in FIREX-AQ biomass burning plumes: the impact of plume concentration on coagulation and OA condensation/evaporation. *Atmos. Chem. Phys.* **2022**, *22* (19), 12803−12825.
(72) Adachi, K.; Dibb, J. E.; Katich, J. M.; Schwarz, J. P.; Guo, H.; Campuzano-Jost, P.; Jimenez, J. L.; Peischl, J.; Holmes, C. D.; Crawford, J. Occurrence, abundance, and formation of atmospheric tarballs from a wide range of wildfires in the western US. *Atmos. Chem. Phys.* **2024**, *24* (19), 10985−11004.
(73) O'Brien, R. E.; Kroll, J. H. Photolytic Aging of Secondary Organic Aerosol: Evidence for a Substantial Photo-Recalcitrant Fraction. *J. Phys. Chem. Lett.* **2019**, *10* (14), 4003−4009.

Downloaded from pubs.acs.org/esthag/article-pdf/60/34/24206/6704211/acs.est.6c02532.pdf by FORSCHUNGZENTRUM JUELICH user on 26 November 2026

https://doi.org/10.1021/acs.est.6c02532
Environ. Sci. Technol. 2026, 60, 24206−24216